The Synergistic Effect Accelerates the Oxygen Reduction/Evolution Reaction in a Zn-Air Battery

Yidan Zhang[1], Youmin Guo[1]*, Tao Liu[1], Fuxu Feng[1], Chunchang Wang[1], Haibo Hu[1], Mingzai Wu[1], Meng Ni[2] and Zongping Shao[3,4]

[1] School of Physics and Materials Science, Anhui University, Hefei, China, [2] Department of Building and Real Estate, The Hong Kong Polytechnic University, Hong Kong, China, [3] State Key Laboratory of Materials-Oriented Chemical Engineering, College of Chemistry and Chemical Engineering, Nanjing University of Technology, Nanjing, China, [4] Department of Chemical Engineering, Curtin University, Perth, WA, Australia

Perovskite oxides are promising electrocatalysts toward oxygen reduction reaction (ORR) and oxygen evolution reaction (OER) due to their abundance and high intrinsic catalytic activity. Here we introduce Ag into $Sm_{0.5}Sr_{0.5}CoO_{3-\delta}$ (SSC) to form a Ag-SSC catalyst by ultrasonication and apply it as the air electrode for a Zn-air battery. It finds that the introduction of Ag into SSC can transform the Ag-SSC into a good bifunctional electrocatalyst toward ORR as well as OER. For instance, a more active half-wave potential with a value of 0.76 V for ORR is obtained at 1,600 rpm, while the OER overpotential is 0.43 V at I = 10 mA cm^{-2}. Further characterization demonstrates that the improved catalyst activity of the Ag-SSC can be assigned to the synergistic effect generated between the Ag and SSC phases. The Zn-air battery with the Ag-SSC as an electrode not only gives a same discharge-charge voltage gap (1.33 V) with that of commercial Pt/C (1.33 V) but also presents an equivalent current efficiency (45.7% for Ag-SSC and 45.3% for Pt/C) at 10 mA cm^{-2}. Moreover, the stability for 110 cycles is better. This result indicates that the Ag-SSC catalyst shows promise for use as a bifunctional electrocatalyst toward OER and ORR.

Keywords: Sr-doped Sm cobaltite perovskite, oxygen reduction reaction, oxygen evolution reaction, silver glue, synergistic effect

INTRODUCTION

The reactions toward the oxygen reduction and oxygen evolution (ORR and OER) play a great role in many conversion systems and energy storage including fuel cells (Xin et al., 2013), Zn-air batteries (Armand and Tarascon, 2008; Chen et al., 2015; Bu et al., 2017), solar fuel synthesis (Gray, 2009), and hydrogen production from water (Walter et al., 2010; Amano et al., 2018; Bu et al., 2019a). Up to now, the commercialization of these renewable energy technologies has been hindered by their sluggish dynamics, so it is urgent to exploit a bifunctional electrocatalyst with superior ORR/OER efficiency and long-term stability. Materials based on noble metals (e.g., Pt, Au) and their alloys (e.g., IrO_2, RuO_2, Pt-Au alloy) are well-known as effective oxygen catalysts for ORR/OER due to their electrocatalytic activities (Chen et al., 2015). However, their large-scale applications are seriously hampered because of their low storage, high cost, and durability (Hong et al., 2015; Zhang et al., 2016). Therefore, researchers have made great efforts to cut down the precious metal loading in noble metal-based catalysts via the use of alloys or a carbon support.

However, the catalytic activities have been simultaneously offset while the noble metal loadings have been decreased. Therefore, it is indispensable to develop bifunctional electrocatalysts that are highly active and stable without precious metals to accelerate their practical application.

Perovskite oxide has been considered as one of the most hopeful alternatives to high efficiency ORR/OER electrocatalysts owing to an extraordinary variability of composition, fascinating physical and chemical properties, low cost and the fact that it is environmentally benign. However, the direct use of pure perovskites as ORR/OER catalysts is disadvantageous. For instance, the performance is limited by poor electronic conductivity at room temperature (Chen et al., 2015; Gupta et al., 2016) because electrocatalysis requires electrons to flow efficiently through the electrodes to produce high currents (Lee et al., 2015; Gupta et al., 2016). Thus, it is crucial to make up for this defect to improve the catalytic efficiency. Nowadays, It has been reported several strategies to improve the catalytic ability of perovskite oxides for ORR/OER, such as defect introduction (Wang et al., 2017), surface modification (Lin et al., 2019), nanostructure optimization (Jung et al., 2016), as well as composite material preparation (Xu et al., 2015; Zhao et al., 2017; Bu et al., 2019b). For example, Zhang et al. indicated that substituting Mg or Fe into the B-site of perovskite with the formation of $LaNi_{0.85}Mg_{0.15}O_3$ and $LaNi_{0.8}Fe_{0.2}O_3$ could enhance the ORR/OER activity of $LaNiO_3$ (Du et al., 2014; Zhang et al., 2015). Zhou and Sunarso proved that the cubic $LaNiO_3$ perovskite showed higher ORR/OER activity by quenching $LaNiO_3$ oxide at different temperatures (Zhou and Sunarso, 2013). Jung et al. compounded a La-doped $Ba_{0.5}Sr_{0.5}Co_xFe_{1-x}O_{3-\delta}$ nanosized particle of 50 nm exhibiting good excellent ORR/OER performance (Jung et al., 2016). To address the issue of low electronic conductivity, some reports tried to add precious metal elements into perovskite oxides, such as platinum (Ho et al., 2011). For instance, Chen et al. compounded ∼1 nm Pt non-structural particles onto ∼60 nm sized $CaMnO_3$ nanoparticles. The synthesized materials showed better performance than Pt/C and $CaMnO_3$ alone as a bifunctional electrocatalyst (Han et al., 2014). However, the manufacturing process was very complicated. Therefore, Zhu et al. proposed a simple ultrasonic technique to mix Pt/C and BSCF for obtaining an excellent bifunctional electrocatalyst through the synergistic effect between Pt/C and the BSCF perovskite (Zhu et al., 2014), and the feasibility of this method provides a good idea for our subsequent experiments.

Due to its reasonably high catalytic capacity in alkaline solutions for oxygen reduction and its low cost, Ag has been considered as a competitive ORR catalyst (Park et al., 2015). Therefore, mixing Ag into perovskite oxides for use as electrocatalysts will be a prospective strategy for promoting the catalytic ability of perovskite oxides as well as for lowering the cost of catalysts. As a kind of cathode candidate for a solid oxide fuel cell, $Sm_{0.5}Sr_{0.5}CoO_{3-\delta}$ (SSC) perovskite oxide has shown excellent oxygen reduction ability (Duan et al., 2018) and has also been demonstrated to be a promising electrocatalyst toward ORR and OER by adding Vulcan XC-72R or N-doped graphene as an electron-conducting phase (Velraj and Zhu, 2013;

Bu et al., 2018). Herein, we designed a new type of catalyst slurry for a Zn-air battery by directly adding commercial silver glue into the SSC perovskite powder catalyst by ultrasonication. The composite slurry (Ag-SSC) exhibited much better ORR/OER activities than either Ag glue or SSC alone in alkaline electrolytes. This research gives prominence to the application of coupled perovskite oxide/silver glue for ORR/OER in a Zn-air battery and suggests the generation of a synergistic effect between the silver glue and the SSC.

MATERIALS AND METHODS

We used a sol-gel method that combined EDTA-citrate complexing to synthesize $Sm_{0.5}Sr_{0.5}CoO_{3-\delta}$ (SSC), and the relevant nitrates were used as the raw materials. First, we completely dissolved these raw materials in the required stoichiometric ratio with deionized water. Next, we introduced citric acid and EDTA as complexing agents and controlled the mixed solution pH at ∼8 under the action of ammonia water. After heating the evaporated water, we obtained a transparent black gel. Finally, the gel was pre-fired at 240°C to form a precursor, and the final powder sample was obtained by calcining the precursor in air at 1,000°C.

A mixed homogeneous catalyst ink composite of SSC powders, conductive carbon (Super P Li), Nafion solution (5 wt %) and ethanol was prepared via ultrasonication. The SSC powder and conductive carbon was mixed at a ratio of 1:1, and the Nafion solution and ethanol were mixed at a ratio of 1:10. Another catalyst ink containing the above prepared SSC ink and an appropriate amount of silver glue was sonicated and labeled as Ag-SSC (the mass ratio of Ag was 25%). Before adding the prepared SSC ink, the silver glue was ground in ethanol solution for half an hour. Then, catalyst inks (5 μL) were drop cast onto a polished glassy carbon electrode (GC, 0.196 cm², Pine Research Instrumentation) and dried in air for 2 h at room temperature. To ensure the cleanness of the GC electrode, we pre-polished the GC electrode using a polishing cloth with a 50 nm α-Al_2O_3 slurry followed by sonication in ethanol for 5 min and then rinsing with deionized water. In this work, the SSC catalyst has a loading amount of 0.232 mg_{ox} cm^{-2}, except for the 20 wt% Pt/C and IrO_2 catalysts (their loading amounts are 0.116 mg cm^{-2}) used as reference catalyst inks.

We used a three-electrode cell (Pine Research Instrumentation) with a rotating disk electrode (RDE) measurement to execute electrochemical measurements using a potentiostat (CHI 650E). Ag/AgCl was applied as a reference electrode, platinum wire was utilized as a counter electrode and KOH aqueous solution (0.1 M) was utilized as the electrolyte. Before each test, O_2 was introduced into the KOH solution to obtain an O_2 saturated solution, ensuring the whole test was conducted under an O_2 atmosphere. We recorded cyclic voltammetry (CV) curves for the catalysts between 0.2 and −0.8 V until a stable curve was obtained. The scan rate was 100 mV s^{-1}. We recorded linear sweeping voltammetry (LSV) curves for the ORR tests via use of the RDE at various rotation speeds (2,000, 1,600, 1,200, 800, and 400 rpm) between

0.2 and −0.8 V. The scan rate was set as 5 mV s$^{−1}$. Both CV and LSV were scanned in the negative mode. We investigated the accelerated stability of catalysts at 1,600 rpm for one thousand cycles through a potential cycle. The scan rate was 100 mV s$^{−1}$, and the potential was changed from 0.2 to −0.8 V. During the reaction for oxygen evolution, LSV curves for the catalysts were recorded. The scan rate was 5 mV s$^{−1}$, and the potential was scanned in positive mode from 0.2 to 0.1 V. In this study, we converted all potentials from vs. Ag/AgCl to the reversible hydrogen electrode (RHE) scale.

The electrochemical test on a zinc-air battery was conducted at room temperature with Zn plate as an anode. A 1 cm^2 catalyst coated carbon paper was applied as an air electrode, while a 6 M KOH solution containing 0.2 M Zn(Ac)$_2$ was utilized as an electrolyte. Before the test, the prepared Ag-SSC catalyst slurry was drop cast onto carbon paper with an amount of 1 mg cm$^{−2}$.

The crystallization of the SSC powder was measured by X-ray powder diffraction (XRD, Bruker AXS D8 Advance), which scanned from 20 to 80° with Cu Kα radiation. The microstructure of the catalysts was characterized by scanning electron microscopy (SEM, Hitachi S-4800) equipped with X-ray energy dispersive spectroscopy (EDX), with the accelerating voltage set as 5 kV. The specific surface area of the samples was measured by the Brunauer-Emmett-Teller (BET) method using nitrogen adsorption and desorption isotherms on a Micromeritics ASAP 2020 system. X-ray photoelectron spectroscopy (XPS, Thermo-Fisher ESCALAB 250Xi), which scanned with a Mg Kα achromatic X-ray source, was used to identify the chemical compositions and surface element states of the samples.

RESULT AND DISCUSSION

The Ag-SSC composite as well as SSC were characterized by XRD scanning from 20 to 80°. As presented in **Figure 1**, sharp and intense diffraction peaks suggested that a well-crystallized phase of SSC was synthesized at 1,000°C. The characteristic reflections for the SSC were observed at 2θ = 23.4, 33.33, 41.08, 47.91, 53.89, 59.65, and 69.99° corresponding to the lattice planes of (100), (110), (111), (200), (210), (211), and (220), respectively. All the peaks shifted to higher 2θ values compared with SrCoO$_3$ (JCPDS file no. 38-1148), indicating that a fraction of the larger Sr^{2+} ions (1.12 Å) was replaced by smaller Sm^{3+} ions (0.96 Å). The XRD patterns for SSC and Ag-SSC were further analyzed by Rietveld refinement. The results showed that the synthesized SSC had a space group of I4/mmm. The values for *a, b,* and *c* were found to be 7.605, 7.605, and 15.195 Å, respectively. The corresponding factor of R$_b$ was 2.45%, confirming the high reliability of the refinement results. After mixing the silver glue, the resulting Ag-SSC composite showed four new diffraction peaks due to Ag, which proved the existence of silver.

The SEM morphology of the Ag-SSC catalyst is displayed in **Figure 2**. The Ag particle was fully distributed into the SSC nanoparticles with sizes of 1∼10 μm (**Figure 2a**). However, the Ag particle had an irregular shape (**Figure 2a**), and the distribution of Ag in the SSC particles was demonstrated to

be uneven (**Figure 2c**), which will adversely affect the activity of the composite catalyst (Guo et al., 2010; Park et al., 2015; Wang et al., 2018). In addition, the content of Ag in Ag-SSC was calculated based on the X-ray energy dispersive spectroscopy (EDX) results and listed in **Table 1**. The content of Ag in Ag-SSC was approximately 25.21 wt % ± 1.83%, which was in line with the ideal design value of 25% in general. The Brunauer-Emmett-Teller (BET) surface area of the SSC was 6.452 m^{2}g$^{−1}$ calculated from N$_2$ isotherms at 77 K.

Figure 3A shows the cyclic voltammetry (CV) tests for SSC, Ag glue, and Ag-SSC catalysts. The peak voltages for SSC, Ag glue, and Ag-SSC were 0.446, 0.432, and 0.560 V, respectively. Obviously, the Ag-SSC exhibited the highest peak voltage among these catalysts, which proved an increased electrocatalytic capacity for ORR due to the addition of Ag glue. To prove this view, we also measured the linear sweeping voltammetry (LSV) curves for all three catalysts. As demonstrated in **Figure 3B**, Ag-SSC presented not only a more positive half-wave potential at 0.76 V but also a higher limited I = 4.87 mA cm$^{−2}$ at 1,600 rpm than that of Ag glue alone and SSC alone (0.53 V/4.92 mA cm$^{−2}$ for Ag glue and 0.55 V/4.39 mA cm$^{−2}$ for SSC), which was similar to that obtained for the benchmark Pt/C catalyst (0.83 V/5.37 mA cm$^{−2}$). This result further indicated that the addition of Ag improved the catalytic ability of SSC for ORR.

We further used the Koutecky-Levich equation to evaluate the ORR kinetics of various catalysts. Through Equation (1), the electron transfer number (n) during the ORR can be calculated (Xiong et al., 2010; Wang et al., 2016):

$$\frac{1}{J} = \frac{1}{J_K} + \frac{1}{J_L} = \frac{1}{nFkC^0} + \frac{1}{0.62nFD_{O_2}^{2/3}v^{-1/6}C^0w^{1/2}} \quad (1)$$

where *w* is the electrode rotating rate; *v* is the kinematic viscosity of the electrolyte via 0.1 M KOH (0.01 cm^2 s$^{−1}$); *J, J$_K$* and *J$_L$* are, respectively, the measured current density, kinetic density and diffusion-limiting current density; *F* is the Faradic constant, 96,485 C mol$^{−1}$; *D$_{O_2}$* represents the oxygen diffusion coefficient via 0.1 M KOH solution (1.9 × 10$^{−5}$ cm^2 s$^{−1}$); *C^0* represents the oxygen bulk concentration (1.1 × 10$^{−6}$ mol cm$^{−3}$); and *k* represents the electron transfer rate constant. From the K-L plots for Ag-SSC fixed at 0.55, 0.60, and 0.65 V (**Figure 3C**), the data show that the transferred electron number approached 4. This result effectively indicated that the ORR process was almost carried out by a four-electron path under the action of the Ag-SSC catalyst in the alkaline electrolyte, suggesting that an advantageous one-step four-electron ORR process with the formation of H$_2$O directly occurred for the Ag-SSC catalyst according to the following equation:

$$O_2 + 4e^- + 4H^+ \rightarrow 2H_2O \quad (2)$$

In fact, there is another reaction pathway in the ORR process: O$_2$ first incurs a two-electron reduction to H$_2$O$_2$ and then continues

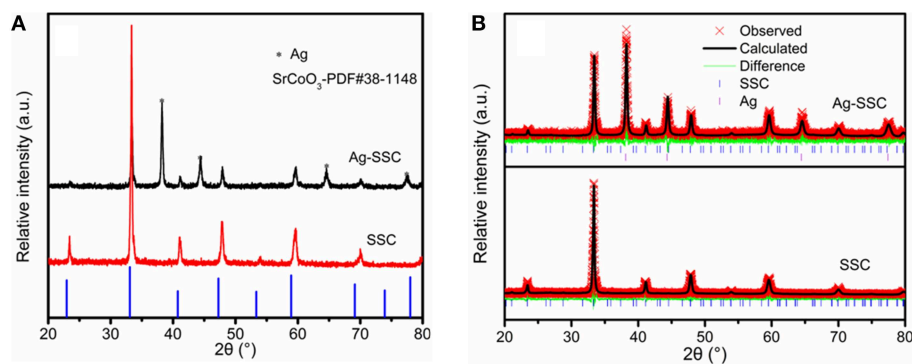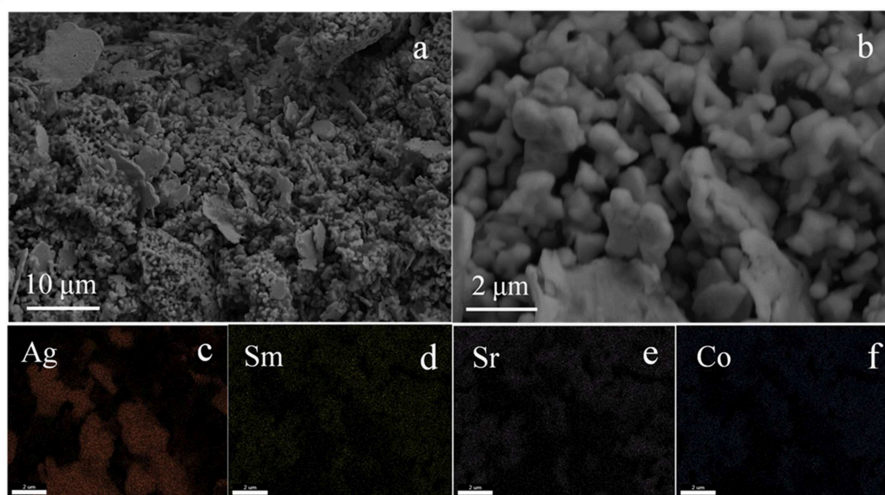**FIGURE 1 |** XRD patterns **(A)** and Rietveld refinement results **(B)** of the SSC and Ag-SSC.


FIGURE 2 | SEM images of Ag-SSC composite **(a,b)** and the corresponding element mappings of Ag **(c)**, Sm **(d)**, Sr **(e)**, Co **(f)**.

TABLE 1 | The X-ray energy dispersive spectroscopy (EDX) results of Ag-SSC.

Element	Weight %	Atomic %	Error %
Ag	25.21	6.90	1.83
Sm	16.05	3.13	4.58
Sr	7.85	2.76	4.05
Co	11.79	5.94	3.87
Others	39.10	81.27	7.89

to an extra two-electron reduction to H_2O. This reaction can be described as follows (Ahmed et al., 2011):

$$O_2 + 2e^- + 2H^+ \rightarrow H_2O_2 \qquad (3)$$

$$H_2O_2 + 2e^- + 2H^+ \rightarrow 2H_2O \qquad (4)$$
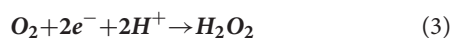
To further obtain kinetic information for the ORR, we recorded the Tafel plots for the different catalysts. From **Figure 3D**, the Tafel plots for SSC, Ag glue, and Ag-SSC were 103.37, 70.30,

and $44.60 \, \text{mV dec}^{-1}$, respectively. These results demonstrated that Ag-SSC had an exceptional ORR activity. The reason for the enhancement for the Ag-SSC catalyst will be discussed later.

The cycle stability is an important performance indicator that determines whether an electrocatalyst is practical. Herein, the stability of the SSC, Ag glue and Ag-SSC were verified by an accelerated aging test. As shown in **Figure 4**, the three catalyst slurries were subjected to 1,000 continuous potential cycles for obtaining a new LSV curve. The experimental settings were the same as that used in the above investigation. The obtained half-wave potential losses of the SSC, Ag glue, and Ag-SSC were $\sim$12, $\sim$36, and $\sim$23 mV, respectively. This obviously showed that the stability of Ag glue alone was bad, similar to the stability of the Pt/C catalyst (Zhu et al., 2015). Even if the SSC catalyst showed the best stability, its catalytic activity was too poor for practical application. After mixing Ag glue into the SSC oxide, the stability of the Ag-SSC composite was much higher than that of Ag glue and the catalytic activity was enhanced substantially. This result indicated that introducing Ag glue
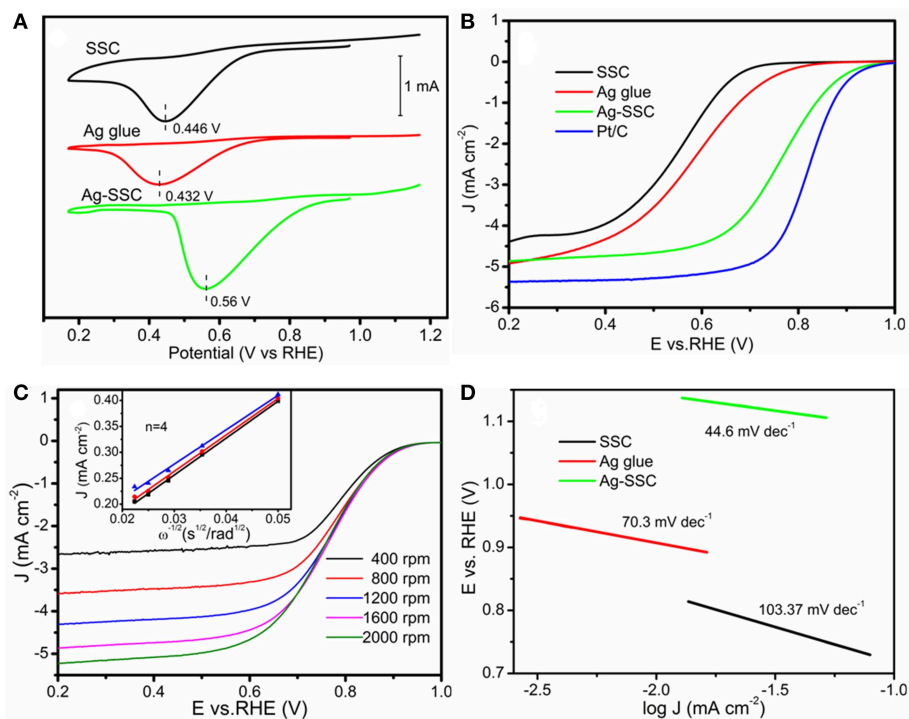
FIGURE 3 | ORR CV curves of SSC, Ag glue, and Ag-SSC catalyst in an O_2-saturated 0.1 M KOH solution at a scan rate of 100 mV s^{-1} (A). LSV curves of SSC, Ag glue, and Ag-SSC catalyst in an O_2-saturated 0.1 M KOH solution at a scan rate of 5 mV s^{-1} at 1,600 rpm (B). LSV curves of Ag-SSC catalyst in an O_2-saturated 0.1 M KOH solution at a scan rate of 5 mV s^{-1} at 400~2,000 rpm and K–L plots for Ag-SSC at 0.55, 0.60, and 0.65 V (C). Tafel plots of SSC, Ag glue, and Ag-SSC (D).
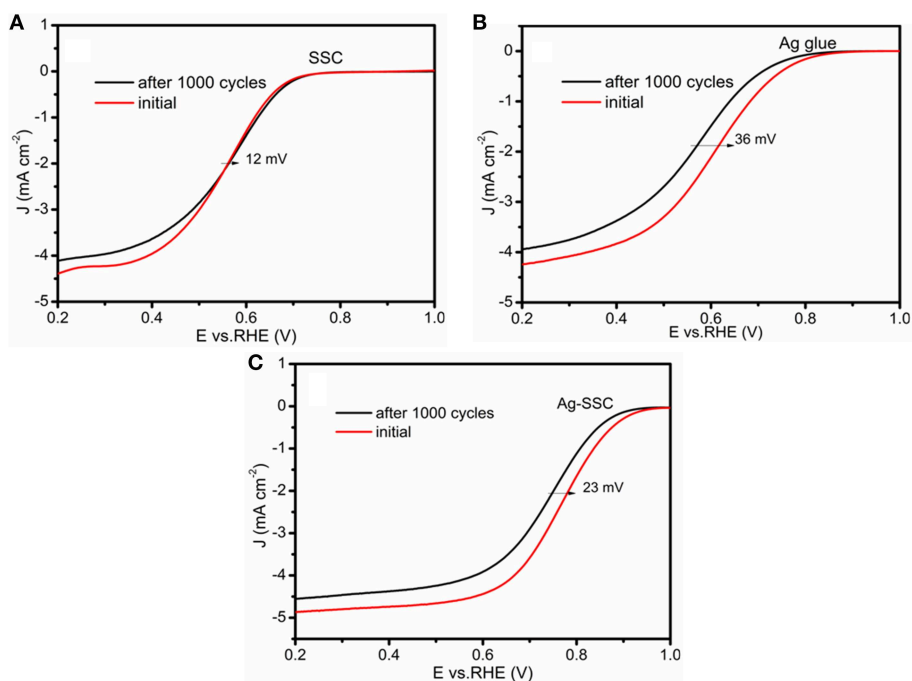

FIGURE 4 | ORR LSV curves of SSC (A), Ag glue (B), and Ag-SSC (C) at 1,600 rpm at a scan rate of 100 mV s^{-1} in an O_2-saturated 0.1 M KOH solution before and after accelerated aging test.
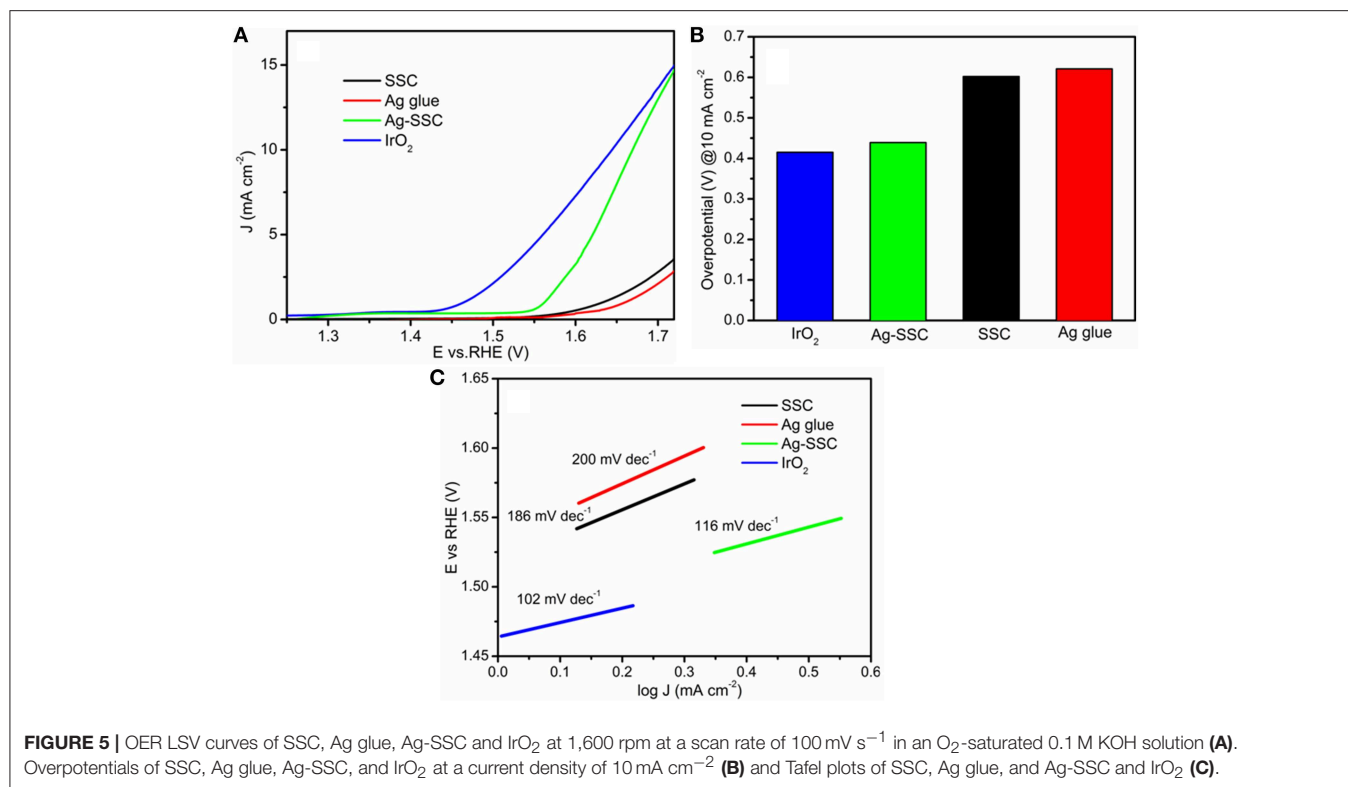
FIGURE 5 | OER LSV curves of SSC, Ag glue, Ag-SSC and IrO$_2$ at 1,600 rpm at a scan rate of 100 mV s^{-1} in an O$_2$-saturated 0.1 M KOH solution **(A)**. Overpotentials of SSC, Ag glue, Ag-SSC, and IrO$_2$ at a current density of 10 mA cm^{-2} **(B)** and Tafel plots of SSC, Ag glue, and Ag-SSC and IrO$_2$ **(C)**.

TABLE 2 | Oxygen electrode activities of SSC, Ag glue and Ag-SSC.

	ORR@-3 mA cm^{-2}	OER@10 mA cm^{-2}	ΔE
SSC	0.50 V	1.83 V	1.33 V
Ag glue	0.54 V	1.85 V	1.31 V
Ag-SSC	0.73 V	1.66 V	0.93 V

into SSC oxide could improve its catalytic activity as well as the stability.

To discover whether the catalyst has bifunctional performance or not, we further tested the OER activity by RDE. **Figure 5A** displays the LSV curves for the OER on SSC, Ag glue, Ag-SSC, and IrO$_2$ at 1,600 rpm. As expected, the Ag-SSC catalyst showed better OER performance than either the Ag glue or SSC catalyst alone. For instance, the onset potentials for SSC, Ag glue, and Ag-SSC were 1.59, 1.58, and 1.54 V, respectively. Meanwhile, Ag-SSC showed a current density that was very close to that obtained for IrO$_2$. The overpotential of the Ag-SSC catalyst was 0.43 V when the current density was 10 mA cm^{-2}, which was smaller than the overpotential of SSC (0.60 V) and Ag glue (0.62 V) alone and approached that of IrO$_2$ (0.40 V) **(Figure 5B)**. This result proved that Ag-SSC also had an active OER activity. In addition, the Tafel slopes were calculated to obtain more kinetic information for the OER and are given in **Figure 5C**. The Tafel slopes for SSC, Ag glue, Ag-SSC and IrO$_2$ were 186, 200, 116, and 102 mV dec^{-1}, respectively. Moreover, the potential difference (ΔE) was calculated at a constant OER current of 10 mA cm^{-2} and ORR

current of −3 mA cm^{-2}, as shown in **Table 2**. The ΔE values were 1.33, 1.31, and 0.93 V for SSC, Ag gluem, and Ag-SSC, respectively. This result obviously demonstrated that ΔE was decreased when Ag was introduced into the SSC perovskite oxide.

According to the above electrochemical results, we discovered that the Ag-SSC composite catalyst had higher OER and ORR catalytic ability than the one-component Ag and SSC perovskite oxide, which indicated that there was a certain synergistic effect at play in the Ag-SSC composite (Zhu et al., 2014). Therefore, the chemical states for Ag and Co in the Ag-SSC composite were detected by XPS. Both Ag glue alone and the Ag-SSC composite exhibited two major peaks with binding energy values at 374.35, 368.35 eV and 374.55, 368.55 eV, respectively **(Figure 6A)**. The spin energy difference in these data was 6 eV, which was consistent with the reported data (Zhang et al., 2016). However, the Ag 3d peak for Ag-SSC showed a slight shift to higher binding energy, indicating that interaction of the perovskite oxide with Ag leads to the transfer of electrons from Ag to SSC (Hong et al., 2015). The Co 2p$_{3/2}$ core spectra for SSC and Ag-SSC are shown in **Figure 6B**. From the fitted curve, the valence of Co in SSC was determined to be between +2 and +3, and the Co^{2+} area ratio was 54%, while in the Ag-SSC structure, the average Co value was close to +2, and the Co^{2+} area ratio was 66%, which was lower than that of Co in the SSC, which indicated that the electronic structure of Co in the Ag-SSC composite was changed due to the action of the Ag (Bu et al., 2018). **Figure 7** presents a schematic for the electron transfer in the Ag-SSC composite. We consider that the surface electronic transfer in the Ag-SSC composite was optimized by
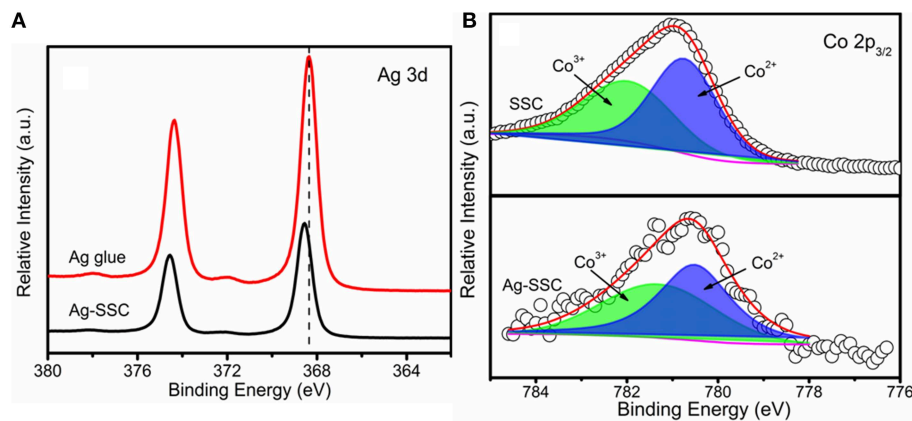
FIGURE 6 | XPS spectra of Ag 3d **(A)** and Co 2p$_{3/2}$ **(B)**.
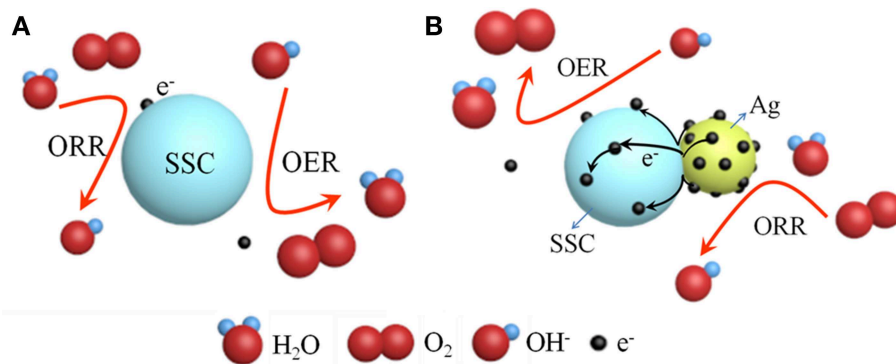

FIGURE 7 | Schematic representation of SSC **(A)** and electron transfer in Ag-SSC composite **(B)** for ORR/OER.

adding Ag into the SSC perovskite oxide, thereby leading to an increased ORR activity. A similar effect of the electron transfer effect has also been previously reported in other systems (Liu and Mustain, 2013; Han et al., 2014; Wang et al., 2018).

To demonstrate the practical use of the Ag-SSC composite, rechargeable Zn-air batteries were assembled with Ag-SSC applied as an air electrode material. **Figure 8A** shows the discharge polarization curves and power densities for our laboratory-made Zn-air battery. The discharge voltage of the Ag-SSC cathode in the battery was 0.98 V at a current density of 50 mA cm^{-2} during the discharge process, which was more inferior to that of a Pt/C cathode (1.06 V) in the same test condition. The peak power density for the Ag-SSC reached 104.46 mW cm^{-2} at 0.65 V, which was slightly smaller than the density of a commercial Pt/C catalyst (113.88 mW cm^{-2}). Based on these data, we consider that the activity of Ag-SSC was slightly inferior to that of the Pt/C electrode, although it showed promising catalytic activity toward OER and ORR. The possible reason for this phenomenon is the uneven distribution of Ag glue in the SSC, resulting in an inability to perform a complete electron transfer between the two phases, thereby reducing the synergistic efficiency.

As we know, for rechargeable metal-air batteries, superior stability for the catalyst is an indispensable condition for an oxygen catalyst; therefore, the operation stability of Ag-SSC for the air electrode of a Zn-air battery was investigated (Zhao et al., 2018). **Figures 8B–E** shows the galvanostatic discharge-charge cycling curves at I = 10 mA cm^{-2} for the Zn-air battery with each cycle being 20 min. It could be seen that under the same test conditions, the Ag-SSC catalyst as a cathode material had a stability property that was similar to that found for the Pt/C catalyst. At the beginning of the loop test, the charge and discharge potentials for the Ag-SSC cathode were 2.35 and 1.18 V, respectively **(Figure 8D)**, and a high voltaic efficiency of 50.2% was obtained, which exceeded that found for the commercial Pt/C catalyst (2.37/1.15 V, 48.5%) **(Figure 8E)**. After 110 cycles, the charge and discharge potentials for Ag-SSC were 2.45/1.12 V and the corresponding values for Pt/C were 2.43/1.10 V. The high voltaic efficiency for Ag-SSC was reduced to 45.7%, while that for Pt/C was decreased to 45.3%. These results revealed that the Ag-SSC cathode had a better long-term cycling stability, even better than a commercial Pt/C cathode. Thus, we conclude that the Ag-SSC composite is an effective catalyst material for use in a rechargeable Zn-air battery.
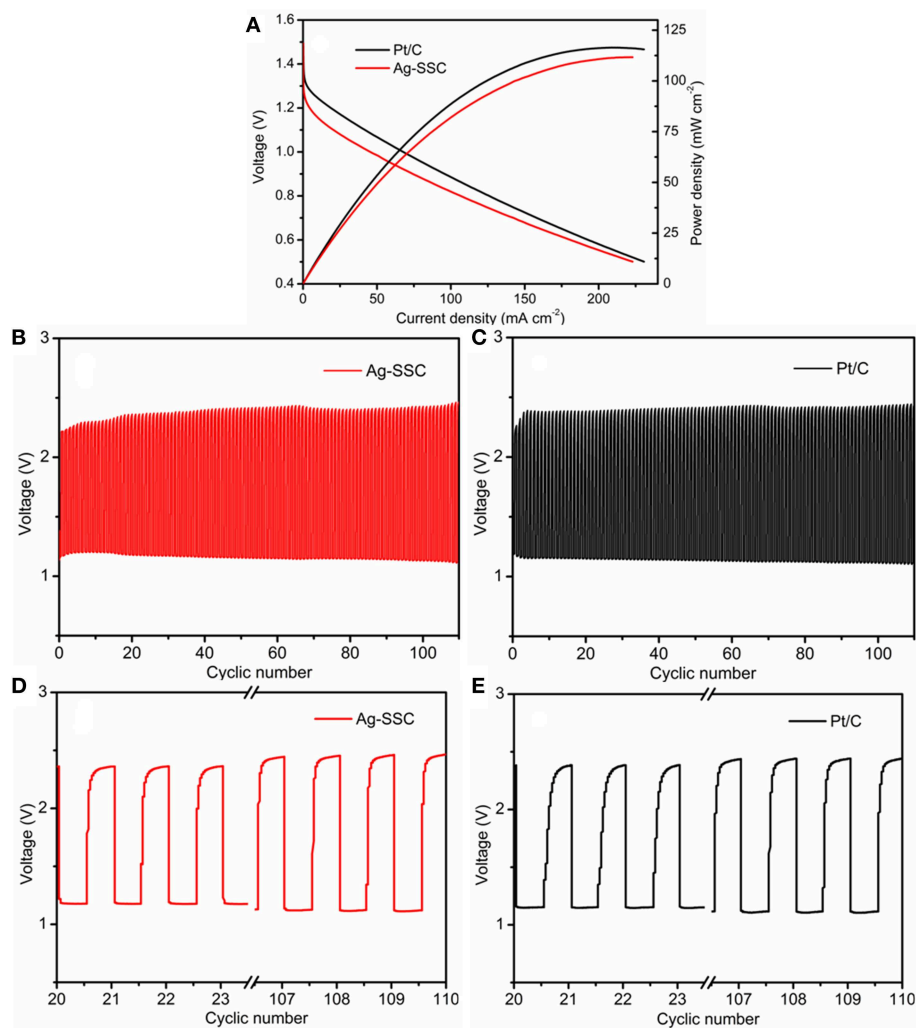
FIGURE 8 | Discharge polarization curve and power density of rechargeable Zn–air battery **(A)**. Galvanostatic discharge-charge cycling curves for Ag-SSC **(B)** and Pt/C **(C)** at $10\,mA\,cm^{-2}$ at different cycles, and comparison of the before and after cycles for Ag-SSC **(D)** and Pt/C **(E)**.

CONCLUSION

In this study, we reported a promising air electrode for a Zn-air battery prepared through simple ultrasonic mixing of Ag glue with a $Sm_{0.5}Sr_{0.5}CoO_{3-\delta}$ (SSC) perovskite oxide. This composite catalyst slurry was demonstrated to show better ORR performance and OER performance than either the SSC or Ag glue alone, which indicates the existence of a synergistic effect between the Ag and SSC phases. According to XPS spectra, we believe that there is electron transfer between the Ag and Co elements. Finally, using the Ag-SSC composite material as an air electrode, a rechargeable Zn-air battery was assembled, which showed a discharge-charge voltage gap similar to that obtained for a Zn-air battery using commercial Pt/C as the air electrode (1.33 V, 1.32 V for Pt/C). In addition, our assembled Zn-air battery showed a high current efficiency (45.7%, 45.3% for Pt/C) at

$10\,mA\;cm^{-2}$, as well as a better cycle stability after 110 cycles. Finally, these experiments showed that our designed bifunctional electrocatalyst has good prospects for application in Zn-air batteries.

DATA AVAILABILITY

All datasets generated for this study are included in the manuscript and/or the supplementary material.

AUTHOR CONTRIBUTIONS

YG contributed conception and design of the manuscript. YZ conducted an experiment and wrote the first draft of the manuscript. All authors contributed

REFERENCES

Ahmed, M. S., Jeong, H., You, J.-M., and Jeon, S. (2011). Electrocatalytic reduction of dioxygen at a modified glassy carbon electrode based on Nafion®-dispersed single-walled carbon nanotubes and cobalt–porphyrin with palladium nanoparticles in acidic media. *Electrochim. Acta* 56, 4924–4929. doi: 10.1016/j.electacta.2011.02.090

Amano, F., Shintani, A., Mukohara, H., Hwang, Y.-M., and Tsurui, K. (2018). Photoelectrochemical gas–electrolyte–solid phase boundary for hydrogen production from water vapor. *Front. Chem.* 6:598. doi: 10.3389/fchem.2018.00598

Armand, M., and Tarascon, J. M. (2008). Building better batteries. *Nature* 451:652. doi: 10.1038/451652a

Bu, Y., Gwon, O., Nam, G., Jang, H., Kim, S., Zhong, Q., et al. (2017). A highly efficient and robust cation ordered perovskite oxide as a bifunctional catalyst for rechargeable zinc-air batteries. *ACS Nano* 11, 11594–11601. doi: 10.1021/acsnano.7b06595

Bu, Y., Kim, S., Kwon, O., Zhong, Q., and Kim, G. (2019a). A composite catalyst based on perovskites for overall water splitting in alkaline conditions. *ChemElectroChem* 6, 1520–1524. doi: 10.1002/celc.201801775

Bu, Y., Nam, G., Kim, S., Choi, K., Zhong, Q., Lee, J., et al. (2018). A tailored bifunctional electrocatalyst: boosting oxygen reduction/evolution catalysis via electron transfer between N-doped graphene and perovskite oxides. *Small* 14:1802767. doi: 10.1002/smll.201802767

Bu, Y. F., Jang, H., Gwon, O., Kim, S. H., Joo, S. H., Nam, G., et al. (2019b). Synergistic interaction of perovskite oxides and N-doped graphene in versatile electrocatalyst. *J. Mater. Chem. A* 7, 2048–2054. doi: 10.1039/c8ta09919g

Chen, D., Chen, C., Baiyee, Z. M., Shao, Z., and Ciucci, F. (2015). Nonstoichiometric oxides as low-cost and highly-efficient oxygen reduction/evolution catalysts for low-temperature electrochemical devices. *Chem. Rev.* 115, 9869–9921. doi: 10.1021/acs.chemrev.5b00073

Du, Z., Yang, P., Wang, L., Lu, Y., Goodenough, J. B., Zhang, J., et al. (2014). Electrocatalytic performances of LaNi1−xMgxO3 perovskite oxides as bi-functional catalysts for lithium air batteries. *J. Power Sources* 265, 91–96. doi: 10.1016/j.jpowsour.2014.04.096

Duan, N., Ma, J., Li, J., Yan, D., Chi, B., Pu, J., et al. (2018). High performance cathode-unsintered solid oxide fuel cell enhanced by porous Bi1.6Er0.4O3 (ESB) interlayer. *Int. J. Hydrogen Energy* 43, 12713–12719. doi: 10.1016/j.ijhydene.2018.03.168

Gray, H. B. (2009). Powering the planet with solar fuel. *Nat. Chem.* 1:7. doi: 10.1038/nchem.141

Guo, J., Hsu, A., Chu, D., and Chen, R. (2010). Improving oxygen reduction reaction activities on carbon-supported ag nanoparticles in alkaline solutions. *J. Phys. Chem. C* 114, 4324–4330. doi: 10.1021/jp910790u

Gupta, S., Kellogg, W., Xu, H., Liu, X., Cho, J., and Wu, G. (2016). Bifunctional perovskite oxide catalysts for oxygen reduction and evolution in alkaline media. *Chem. Asian J.* 11, 10–21. doi: 10.1002/asia.201500640

Han, X., Cheng, F., Zhang, T., Yang, J., Hu, Y., and Chen, J. (2014). Hydrogenated uniform Pt clusters supported on porous CaMnO3 as a bifunctional electrocatalyst for enhanced oxygen reduction and evolution. *Adv. Mater.* 26, 2047–2051. doi: 10.1002/adma.201304867

Ho, V. T. T., Pan, C.-J., Rick, J., Su, W.-N., and Hwang, B.-J. (2011). Nanostructured Ti0.7Mo0.3O2 support enhances electron transfer to Pt: high-performance catalyst for oxygen reduction reaction. *J. Am. Chem. Soc.* 133, 11716–11724. doi: 10.1021/ja2039562

Hong, W. T., Risch, M., Stoerzinger, K. A., Grimaud, A., Suntivich, J., and Shao-Horn, Y. (2015). Toward the rational design of non-precious transition metal oxides for oxygen electrocatalysis. *Energy Environ. Sci.* 8, 1404–1427. doi: 10.1039/c4ee03869j

Jung, J.-I., Risch, M., Park, S., Kim, M. G., Nam, G., Jeong, H.-Y., et al. (2016). Optimizing nanoparticle perovskite for bifunctional oxygen electrocatalysis. *Energy Environ. Sci.* 9, 176–183. doi: 10.1039/c5ee03124a

Lee, D.-G., Gwon, O., Park, H.-S., Kim, S. H., Yang, J., Kwak, S. K., et al. (2015). Conductivity-dependent completion of oxygen reduction on oxide catalysts. *Angew. Chem. Int. Ed.* 54, 15730–15733. doi: 10.1002/anie.201508129

Lin, H., Liu, P., Wang, S., Zhang, Z., Dai, Z., Tan, S., et al. (2019). A highly efficient electrocatalyst for oxygen reduction reaction: three-dimensionally ordered macroporous perovskite LaMnO3. *J. Power Sources* 412, 701–709. doi: 10.1016/j.jpowsour.2018.12.005

Liu, Y., and Mustain, W. E. (2013). High stability, high activity Pt/ITO oxygen reduction electrocatalysts. *J. Am. Chem. Soc.* 135, 530–533. doi: 10.1021/ja307635r

Park, S.-A., Lim, H., and Kim, Y.-T. (2015). Enhanced oxygen reduction reaction activity due to electronic effects between Ag and Mn3O4 in alkaline media. *ACS Catal.* 5, 3995–4002. doi: 10.1021/acscatal.5b00495

Velraj, S., and Zhu, J. H. (2013). Sm0.5Sr0.5CoO3−δ – a new bi-functional catalyst for rechargeable metal-air battery applications. *J. Power Sources* 227, 48–52. doi: 10.1016/j.jpowsour.2012.11.031

Walter, M. G., Warren, E. L., McKone, J. R., Boettcher, S. W., Mi, Q., Santori, E. A., et al. (2010). Solar water splitting cells. *Chem. Rev.* 110, 6446–6473. doi: 10.1021/cr1002326

Wang, M., Hou, Y., Slade, R. C. T., Wang, J., Shi, D., Wexler, D., et al. (2016). Core-shell Co/CoO integrated on 3D nitrogen doped reduced graphene oxide aerogel as an enhanced electrocatalyst for the oxygen reduction reaction. *Front. Chem.* 4:36. doi: 10.3389/fchem.2016.00036

Wang, Q., Xue, Y., Sun, S., Li, S., Miao, H., and Liu, Z. (2017). La0.8Sr0.2Co1-xMnxO3 perovskites as efficient bi-functional cathode catalysts for rechargeable zinc-air batteries. *Electrochim. Acta* 254, 14–24. doi: 10.1016/j.electacta.2017.09.034

Wang, X., Ge, L., Zhu, Y., Dai, J., Zhou, W., and Shao, Z. (2018). Silver-perovskite hybrid electrocatalysts for oxygen reduction reaction in alkaline media. *J. Electrochem. Soc.* 165, H524–H529. doi: 10.1149/2.1131809jes

Xin, L., Zhang, Z., Wang, Z., Qi, J., and Li, W. (2013). Carbon supported Ag nanoparticles as high performance cathode catalyst for H2/O2 anion exchange membrane fuel cell. *Front. Chem.* 1:16. doi: 10.3389/fchem.2013.00016

Xiong, W., Du, F., Liu, Y., Perez, A., Supp, M., Ramakrishnan, T. S., et al. (2010). 3-D carbon nanotube structures used as high performance catalyst for oxygen reduction reaction. *J. Am. Chem. Soc.* 132, 15839–15841. doi: 10.1021/ja104425h

Xu, Y., Tsou, A., Fu, Y., Wang, J., Tian, J.-H., and Yang, R. (2015). Carbon-coated perovskite BaMnO3 porous nanorods with enhanced electrocatalytic perporites for oxygen reduction and oxygen evolution. *Electrochim. Acta* 174, 551–556. doi: 10.1016/j.electacta.2015.05.184

Zhang, D., Song, Y., Du, Z., Wang, L., Li, Y., and Goodenough, J. B. (2015). Active LaNi1-xFexO3 bifunctional catalysts for air cathodes in alkaline media. *J. Mater. Chem. A* 3, 9421–9426. doi: 10.1039/c5ta01005e

Zhang, J., Fu, J., Song, X., Jiang, G., Zarrin, H., Xu, P., et al. (2016). Laminated cross-linked nanocellulose/graphene oxide electrolyte for flexible rechargeable zinc–air batteries. *Adv. Energy Mater.* 6:1600476. doi: 10.1002/aenm.201600476

Zhao, B., Zhang, L., Zhen, D., Yoo, S., Ding, Y., Chen, D., et al. (2017). A tailored double perovskite nanofiber catalyst enables ultrafast oxygen evolution. *Nat. Commun.* 8:14586. doi: 10.1038/ncomms14586

Zhao, C., Jin, Y., Du, X., and Du, W. (2018). *In situ* prepared amorphous FeCoO-Polyaniline/multiwalled carbon nanotube nanohybrids as efficient oxygen evolution catalysts for rechargeable Zn-air batteries. *J. Power Sources* 399, 337–342. doi: 10.1016/j.jpowsour.2018.07.111

Zhou, W., and Sunarso, J. (2013). Enhancing bi-functional electrocatalytic activity of perovskite by temperature shock: a case study of LaNiO3−δ. *J. Phys. Chem. Lett.* 4, 2982–2988. doi: 10.1021/jz401169n

Zhu, Y., Su, C., Xu, X., Zhou, W., Ran, R., and Shao, Z. (2014). A universal and facile way for the development of superior bifunctional electrocatalysts for oxygen reduction and evolution reactions utilizing the synergistic effect. *Chem. Eur. J.* 20, 15533–15542. doi: 10.1002/chem.201403192

Zhu, Y., Zhou, W., Chen, Y., Yu, J., Xu, X., Su, C., et al. (2015). Boosting oxygen reduction reaction activity of palladium by stabilizing its unusual oxidation states in perovskite. *Chem. Mater.* 27, 3048–3054. doi: 10.1021/acs.chemmater.5b00450

Conflict of Interest Statement: The authors declare that the research was conducted in the absence of any commercial or financial relationships that could be construed as a potential conflict of interest.